Annu. Rev. Phys. Chem. 2005. 56:337–67
doi: 10.1146/annurev.physchem.56.092503.141314

First published online as a Review in Advance on January 7, 2005

ULTRAFAST CHEMISTRY: Using Time-Resolved Vibrational Spectroscopy for Interrogation of Structural Dynamics

Erik T.J. Nibbering,[1] Henk Fidder,[2] and Ehud Pines[3]
[1]*Max Born Institut für Nichtlineare Optik und Kurzzeitspektroskopie, D-12489 Berlin, Germany; email: nibberin@mbi-berlin.de*
[2]*Department of Physical Chemistry, Uppsala Universitet, S-751 23 Sweden; email: henk.fidder@fki.uu.se*
[3]*Department of Chemistry, Ben-Gurion University of the Negev, Beer-sheva 84105, Israel; email: epines@bgumail.bgu.ac.il*

Key Words hydrogen and proton transfer, hydrogen bonding and solvation, intramolecular vibrational redistribution and vibrational cooling, anharmonic coupling between vibrational modes, internal conversion

■ **Abstract** Time-resolved infrared (IR) and Raman spectroscopy elucidates molecular structure evolution during ultrafast chemical reactions. Following vibrational marker modes in real time provides direct insight into the structural dynamics, as is evidenced in studies on intramolecular hydrogen transfer, bimolecular proton transfer, electron transfer, hydrogen bonding during solvation dynamics, bond fission in organometallic compounds and heme proteins, *cis-trans* isomerization in retinal proteins, and transformations in photochromic switch pairs. Femtosecond IR spectroscopy monitors the site-specific interactions in hydrogen bonds. Conversion between excited electronic states can be followed for intramolecular electron transfer by inspection of the fingerprint IR- or Raman-active vibrations in conjunction with quantum chemical calculations. Excess internal vibrational energy, generated either by optical excitation or by internal conversion from the electronic excited state to the ground state, is observable through transient frequency shifts of IR-active vibrations and through nonequilibrium populations as deduced by Raman resonances.

1. INTRODUCTION: ULTRAFAST STRUCTURAL DYNAMICS IN CONDENSED-PHASE CHEMISTRY

Chemistry occurs on a large range of timescales. Rearrangements of biomolecular structures, such as protein synthesis in ribosomes, or DNA multiplication, involve a large number of chemical transformations, making the timescales of these processes span on the order of seconds to hours. Bimolecular reaction dynamics in liquid solutions are dominated by relatively slow mutual diffusion (1); typical

timescales are on the order of nanoseconds. Elementary steps in chemistry, such as the dynamical event of a single-bond rearrangement, appear to take place on femtosecond to picosecond timescales [femtochemistry (2)]. Examples of ultrafast chemistry include hydrogen and proton transfer, electron transfer, bond fissions, and *cis-trans* isomerizations. In the case of ultrafast condensed-phase chemistry the dynamics are determined not only by the potential energy surfaces of the reactant-product species. The surrounding solvent also plays a major role in modulating the energy levels of reactants, intermediates, and products, as well as the energy barriers separating these species (3). In addition, the solvent plays the role of donor or acceptor of energy (4), often causing an outcome of chemical reactions different from those for isolated reacting species. Photoinduced chemistry offers the opportunity of triggering the reaction dynamics at a well-defined point in time. Ultrafast spectroscopy has been an exquisite tool to follow chemical reactions in real time after applying such an optical trigger pulse.

Since the development of short-pulsed laser systems, ultrafast chemistry in the condensed phase has been studied mainly using time-resolved electronic spectroscopy. After the ultrashort optical trigger pulse induces a transition to a higher lying electronic state, the evolution of the molecular system is followed either by time-resolved fluorescence emission, or by absorbance changes of a probe pulse tuned to electronic resonances in the near-UV or vis regions of the electromagnetic spectrum. The disadvantage of probing electronic transitions lies in the fact that these are typically strongly broadened owing to coupling to the fluctuating surrounding solvent (5–7). As a result, the relatively featureless transient electronic bands of stimulated emission and excited state absorption contributions often overlap (8), whereas spectral shifting and reshaping caused by solvent reorganization (solvation dynamics) and energy dissipation (vibrational cooling) complicate the situation even more.

More insight into the dynamics of molecular structures may be achieved using ultrafast structurally resolving techniques. Whereas time-resolved X-ray (9) and electron diffraction (10, 11) and X-ray spectroscopy (12) are still rather technologically demanding, recent developments in ultrafast laser technology have enabled the efficient generation of tunable femtosecond laser pulses from the UV to the far-infrared regions of the electromagnetic spectrum (13, 14), making femtosecond vibrational spectroscopy a versatile tool. Since an early example of picosecond infrared (IR) spectroscopy on excited state intramolecular hydrogen transfer (ESIHT) in 1986 (15), the method has mainly been employed on metallocarbonyl compounds (16–19) and heme proteins (20–22). With the availability of sensitive mid-infrared detector arrays it is now possible to fully explore the potential of time-resolved vibrational spectroscopy for gaining insight into transient molecular structures involved in chemical reaction pathways. Until now, optically triggered chemical reaction dynamics has been studied with femtosecond IR spectroscopy on cases as diverse as ESIHT (23, 24), bimolecular proton transfer (25, 26), electron transfer (27–39), hydrogen bonding in solvation dynamics (40–44), photochemistry of small molecules (17, 45–47), bond fission (48–56) and bond

activation (57–60) in organometallic compounds, ligand release in heme proteins (9, 61–64), *cis-trans* isomerization (65–70), and more extensive rearrangements in photochromic switches (71–73). Picosecond resonance Raman spectroscopy has been used in electron transfer studies (74–76) and intramolecular vibrational redistribution studies (77–82). Coherent anti-Stokes Raman spectroscopy (CARS) has been applied to photoinduced dynamics of photochromic switches (83), retinal proteins (84–89), and photoactive yellow protein (90).

We give an overview of recent achievements in time-resolved vibrational spectroscopy of ultrafast condensed-phase chemistry. We first describe the advantages of ultrafast vibrational spectroscopy as a tool to resolve dynamically changing molecular structures. We then present examples of excited state hydrogen transfer, bimolecular proton transfer dynamics, excited state electron transfer, hydrogen bonding in solvation dynamics, bond fission, and isomerization reactions (also see Figure 1). We conclude with a prospective outlook.

2. ULTRAFAST INFRARED AND RAMAN SPECTROSCOPY

Vibrational spectroscopy has several advantages over electronic spectroscopy. Vibrational transitions can often be correlated to specific vibrational motions by inspection of the transition frequencies. In particular the fingerprint region offers a wealth of structural information. From identification of these fingerprint vibrational modes, conclusions can be drawn on specific structural motifs in the molecules. Vibrational transitions have bandwidths typically smaller (10–20 cm^{-1}) than those from electronic transitions (typically 200–2000 cm^{-1}), due to longer transverse dephasing times [the exception to the rule: O–H/O–D stretching vibrations in hydrogen-bonded hydroxyl groups (91)]. It is thus less probable that different transition bands overlap in vibrational spectroscopy than in electronic spectroscopy. In addition, small molecular species may always be probed through their vibrations, whereas their electronic transitions often lie in the far-UV (that would normally be hidden underneath the solvent bands). Major disadvantages of vibrational spectroscopy on the other hand are the inherent lower cross sections of vibrational transitions, and the frequent overlap of the absorption bands with those of the solvent. The mismatch in cross sections of electronic and vibrational transitions often leads to experimental situations having high excitation densities of samples with absorber concentrations on the order of 1–20 mM (with often high optical densities for the electronic transitions of OD = 1–2). Deformation of laser pulses while propagating through the samples, probe molecule aggregation and sample degradation have to be checked when performing ultrafast mid-infrared experiments. Time-resolved Raman experiments often are hampered by unwanted fluorescent emission of the molecules under study, or of impurities in the samples.

In the case that specific vibrational marker modes of reactant, intermediate, and product states are identified, one can follow the outcome of the photoinduced reaction by inspection of the transitions of these marker modes. Site-specific

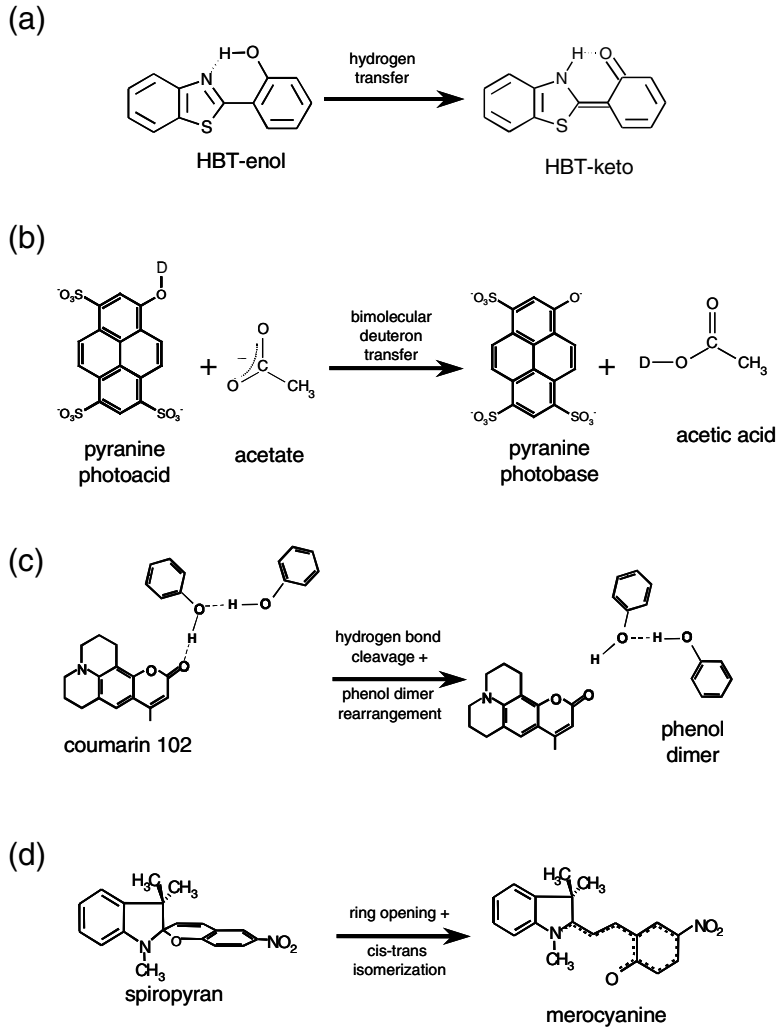

Figure 1 Examples of chemical reaction dynamics studied with ultrafast infrared spectroscopy, as explained in the text: (*a*) excited state intramolecular hydrogen transfer of HBT; (*b*) bimolecular acid-base neutralization reaction between pyranine and acetate; (*c*) hydrogen bond rearrangement after optical excitation of C102-$(phenol)_2$ complexes; (*d*) ring-opening and *cis-trans* isomerization of 6-nitro-BIPS.

information is obtained in the case of vibrational marker modes that involve nuclear motions of specific molecular side groups. When vibrational normal modes are involved in nuclear motions of extended parts of the molecules, a direct structural insight is usually not obtained. Isotopic substitution reveals the involvement of certain nuclei in the vibrational motions. When, in comparing the experimentally observed vibrational mode pattern with predictions from quantum chemical calculations, a full correspondence is possible, the three-dimensional structure is derivable. Current quantum chemical calculational routines, such as density functional theory (92), allow for the estimation of the electronic ground state structure of medium-sized molecules. For intermediate and product states in electronic excited states, however, reliable results can be obtained with the routine of ab initio complete active space self-consistent field (CASSCF) (93), albeit for mid-size molecules not much larger than 20 atoms. New developments in numerical procedures, such as time-dependent density functional theory (TD-DFT) (94), may prove beneficial in the estimation of larger molecular structures in electronic excited states.

Polarization-dependent UV/vis-pump IR-probe spectroscopy provides insight into the relative angles between the optical and IR transition dipole moments. From these experiments angular information on transient species is obtainable (20, 61). Because of sensitivity reasons (electronic transitions typically have cross sections 100–1000 times stronger than vibrational transitions), often high energy densities of the electronic pump pulses are used. Care should be taken when considering polarization-dependent measurements because of the effects of finite bleaching, where the ground state bleaching of the sample is significant (a total bleached fraction on the order of 0.1 or higher) (21). When the vibrational marker mode is a local mode, a direct link is present between the optical transition dipole moment and the vector of the chemical bond modulated by the vibration. More often, for delocalized normal modes one must rely on comparison between the experimentally found angular information and quantum chemical calculations (64, 95).

In the most basic situation the reaction kinetics are deducible by inspection of vibrational marker modes of reactants, intermediates, and products. The rise and decay behavior of specific vibrational marker bands indicate the formation and disappearance of reactant, intermediate, and product states. Inspection of the spectral shifts and widths of these bands, however, can reveal additional information on local interactions, vibrational energy redistribution, and energy dissipation to the solvent.

Site-specific information is obtainable by inspection of local modes that are affected by local interactions. For instance, it is well known that hydrogen bonding induces marked shifts in O–H, N–H, C=O and C=N bands in the case where these structural functionalities are involved in hydrogen bonding (96). Observation of transient spectral shifts reveals important information on changes in hydrogen bond interactions (weakening/strengthening or even hydrogen bond cleavage).

In polyatomic molecules the vibrational normal modes are usually considered in the harmonic oscillator approximation. In this limit the motions of the vibrational modes are independent of each other. In reality anharmonicity of the vibrational modes cannot be neglected; anharmonicity is typically treated as perturbation to the Hamiltonian in the eigenstate representation of the harmonic oscillator normal modes (97, 98). The first consequence is diagonal anharmonicity, where the energy spacing between the vibrational levels becomes smaller as the corresponding vibrational quantum numbers become higher. Another consequence is that the motions of the vibrational normal modes are no longer independent, as indicated by off-diagonal anharmonicity terms in the Hamiltonian. Let us assume a representation of the vibrational energy eigenstates of a polyatomic molecule with quadratic anharmonicity only (without degenerate states) (66) as:

$$\frac{E}{hc} = \sum_{\mathrm{i}} \tilde{\nu}_{\mathrm{i}} \left(\mathrm{v_i} + \frac{1}{2} \right) + \sum_{i \leq j} x_{ij} \left(\mathrm{v}_i + \frac{1}{2} \right) \left(\mathrm{v}_j + \frac{1}{2} \right), \qquad 1.$$

where ν_i is the harmonic frequency, and $\mathrm{v_i}$ is the vibrational quantum number of mode i, and x_{ij} are the anharmonic coupling constants between modes i and j, which typically have negative values. The transition frequency for a mode k coupled to the other modes $i \neq k$ is then:

$$\frac{E\,(\mathrm{V}_k \rightarrow \mathrm{V}_k + 1)}{hc} = \tilde{\nu}'_k + 2x_{kk}\mathrm{v}_k + \sum_{i \neq k} x_{ik}\mathrm{v}_i; \qquad 2.$$

the first term on the right-hand side of Equation 2 defines the anharmonic correction for the $\mathrm{v}_k \rightarrow \mathrm{v}_k + 1$ transition when the other vibrational modes i are in the ground state ($\mathrm{v}_i = 0$), i.e., the molecule is cold:

$$\tilde{\nu}'_k = \tilde{\nu}_k + 2x_{kk} + \sum_{i \neq k} \frac{x_{ik}}{2}. \qquad 3.$$

The second term on the right-hand side of Equation 2 indicates the influence of the diagonal anharmonicity: The transitions in the vibrational ladder are successively shifted to lower frequencies. The third term on the right-hand side of Equation 2 shows the influence of off-diagonal anharmonicity: when other modes i are highly excited (high quantum number v_i indicates that the molecule is hot, i.e., it has a large internal vibrational energy), the marker mode k exhibits a redshifted transition frequency, even for the fundamental $\mathrm{v}_k = 0 \rightarrow \mathrm{v}_k = 1$ transition. This off-diagonal anharmonicity is explored in multidimensional IR spectroscopic studies (99). Multidimensional IR spectroscopy has mainly been pursued in the elucidation of polypeptide and metallo-carbonyl compounds in the electronic ground state, where the magnitudes of the couplings give structural information, and the dynamics of these couplings reveal the fluctuations of these structures. Only recently has this technique been applied on transient states generated by an electronic pump pulse (69).

A high degree of internal vibrational energy can be generated under different circumstances. For instance, for electronic transitions with a small displacement of Raman-active vibrations most of the electronic transition moment is located in the electronic 0–0 origin transition. The transition could be excited into the higher lying part of the electronic band by tuning the UV/vis-pump pulse where, upon electronic excitation, several Raman-active vibrations also change their vibrational quantum number. When probing an infrared-active marker mode in this electronic excited state, a red-shifted transition frequency is observable for this marker mode as opposed to where it will show up when exciting in the electronic origin. For molecular systems with a large displacement for one or several Raman-active vibrations, the maximum of the absorption band already corresponds to a significant amount of internal vibrational energy. The apparent red-shifted position of the IR-active marker modes already occurs when this excess vibrational energy is only contained in a subset of vibrational modes (e.g., the Raman-active modes that show a large displacement upon electronic excitation). Intramolecular vibrational energy redistribution (IVR) will typically equilibrate this excess energy over all vibrational modes in the molecule (on timescales ranging from below 100 fs to several picoseconds for mid-size molecules) (100). In condensed-phase solutions the energy dissipation to the solvent (cooling) is irreversible, which translates into a blue-shifting behavior of the positions of the vibrational marker modes to the frequency position observable when exciting into the electronic origin transition. Vibrational cooling typically takes place on timescales of several tens of picoseconds (101–103).

When ultrafast internal conversion to other electronic states (reactant ground state, or product states) occurs, typically a substantial amount of—if not all electronic—excitation energy is converted into internal vibrational energy before the energy dissipation to the solvent can be effective. Transiently red-shifted vibrational transitions of fingerprint marker modes have been observed in these cases as well. In the case of an ultrafast internal conversion of the electronic excited state to the ground state on a timescale of a few hundreds of femtoseconds, one would typically observe for the vibrational marker mode a bleach signal corresponding to the location of the marker mode transition of the cold molecule, and red-shifted the vibrational marker mode transition of the hot molecule. Only upon cooling is the disappearance of the red-shifted hot ground state absorption accompanied by a refill of the ground state bleach observable. The magnitude of the refill of the ground state bleach enables an estimation of the quantum yield of this ultrafast internal conversion (IC) process back to the electronic ground state (71–73).

Experimentally, transient IR spectroscopy is performed in a spectrally-resolved configuration. Femtosecond IR parametric devices deliver pulses with bandwidths of 150 cm^{-1} or more (14). In order to observe shifts as small as the linewidths of IR-active vibrations, the IR absorbance change must be measured with a detector after spectral dispersion with a monochromator. As a side effect of this spectral dispersion, ground state bleach signals often appear to grow at negative pulse delay with the dephasing time of the transition. This effect, known as perturbed free induction decay, is a common feature of spectrally-resolved nonlinear pump-probe

spectroscopy of bleached transitions with dephasing times much longer than the time resolution of the experiment (104–106). The time resolution of the experiment is given by the cross correlation between the UV/vis-pump and IR-probe pulse (about 100–200 fs), and is typically dominated by group velocity mismatch in samples with thicknesses of about 100 μm.

In principle the same approach can be followed by probing Raman-active vibrations. In this case the spectral resolution is determined not only by the monochromator through which the spontaneous Raman emission is dispersed, but also by the bandwidth of the gating pulse by which the Raman effect is induced. As a result UV/vis-pump Raman-probe spectroscopy has a temporal resolution of around 1 ps (a compromise between spectral and time resolution) (107). Because of the even weaker cross sections of Raman transitions, resonance enhancement is often used by tuning the gating pulse close to or resonant with an electronic transition of the state that is probed. This has the advantage of isolating Raman bands of the state under inspection for observation. The drawback is that fluorescence resulting from the resonant electronic excitation often inhibits detection of Raman bands in extended spectral ranges. Dedicated Raman detection techniques such as Kerr-gates may suppress this unwanted fluorescence emission (108). CARS, being a coherent technique, does not have this drawback, at the cost of a more complex laser configuration.

Raman spectroscopy offers an additional insight into how chemical reactions evolve. By comparison of the intensities of anti-Stokes and Stokes lines of a particular vibration, it is possible to derive time-dependent changes in the excitation level of this vibration. One can draw conclusions on whether particular modes initially drive a chemical reaction (state transition promoting modes), or only get excited after the transition is made, by taking up the excess energy released by the reaction (accepting modes). In such a way insight is obtained on the energy flow inside a molecular system (IVR) and cooling to the surrounding solvent. Although IR-active transitions exhibit transient frequency shifts due to IVR and cooling as well, it is not easy to deduce transient higher excitation levels of these modes.

3. EXCITED STATE INTRAMOLECULAR HYDROGEN TRANSFER

Hydrogen bonds determine to a substantial extent the microscopic structure of a large variety of molecular systems, ranging from hydrogen-bonding liquids to proteins and DNA. In these structures molecular function often involves hydrogen or proton transfer along preformed hydrogen bonds. The most elementary hydrogen transfer reactions consist of a hydrogen atom H shifting from originally being part of a covalent bond A–H to a new binding site B in the same or a neighboring molecule.

$$\mathrm{A{-}H\cdots B} \rightarrow \mathrm{A\cdots H{-}B} \qquad 4.$$

In the electronic ground state a transfer can be caused by solvent-induced fluctuations of hydrogen-bonded networks. Hydrogen transfer can also be induced after optical excitation. The study of photoinduced ESIHT was pioneered by Weller (109). (For a review of early work on several prototype ESIHT cases, see Reference 110; for a recent overview including ultrafast spectroscopic work, see Reference 111.) Although traditionally these experiments have been interpreted to involve excited state intramolecular proton transfer (ESIPT), in reality the motions of the proton are typically accompanied by rearrangements of the electronic charge densities, and it is more appropriate to describe the observed features as being caused by the net transfer of a hydrogen atom, i.e., ESIHT. Elsaesser & Kaiser reported a pioneering picosecond IR experiment on 2-(2′-hydroxyphenyl)benzothiazole (HBT) (15), where a first direct characterization of local changes of molecular geometries due to hydrogen transfer from the enol to keto state was demonstrated by inspection of IR absorbance changes in the O–H stretching band centred at 3000 cm^{-1} and in the fingerprint region between 1400 and 2000 cm^{-1}. Femtosecond time resolution however, is required to resolve the formation dynamics of the product state. In UV/vis pump-probe experiments, where e.g., stimulated emission from product states is measured, rise times for ESIHT systems ranging from several tens to hundreds of femtoseconds have been found (111).

Femtosecond IR spectroscopy has been reported on the ESIHT enol-keto reaction of HBT (23, 24). Here the C=O stretching marker mode at 1530 cm^{-1}, as well as other fingerprint vibrations, has been monitored after excitation with the UV pump tuned between 310 and 350 nm (see Figure 2). The C=O stretching mode has a transition frequency significantly lower than free C=O vibrations, as the carbonyl group is part of the hydrogen-bonded C–N–H $\cdots$ O=C moiety and because it is part of a larger conjugated π-electronic system. Figure 3 shows the rise of the C=O stretching marker mode delayed by 30–50 fs after UV excitation of the enol state. This result indicates that the keto-state is generated on a 50 fs timescale, hinting at an essentially barrierless excited state potential along the reaction coordinate (23). The transfer dynamics however, appears to be much slower than the period of the O–H stretching vibration of approximately 10 fs. This leads to the conclusion that hydrogen transfer does not involve a simple stretching motion from donor to acceptor groups.

The transient IR spectra of HBT also provide information on IVR and cooling processes (23, 24). During and after hydrogen transfer, the vibronic excess energy originating from the UV pump pulse and from the energy difference between the enol-S_1 and keto-S_1 states is redistributed over numerous intramolecular vibrations and is eventually dissipated to the solvent. If any of the investigated modes is excited to the corresponding $v = 1$ or higher levels, it will immediately give rise to vibrational absorption and stimulated emission from these higher lying levels, and to different signatures in the transient absorbance spectra. The C=O stretching mode, however, only shows minor changes in spectral envelope and integrated absorption as a function of pulse delay (23). This points to a formation of the C=O stretching mode in its $v = 0$ ground state without passing through $v = 1$

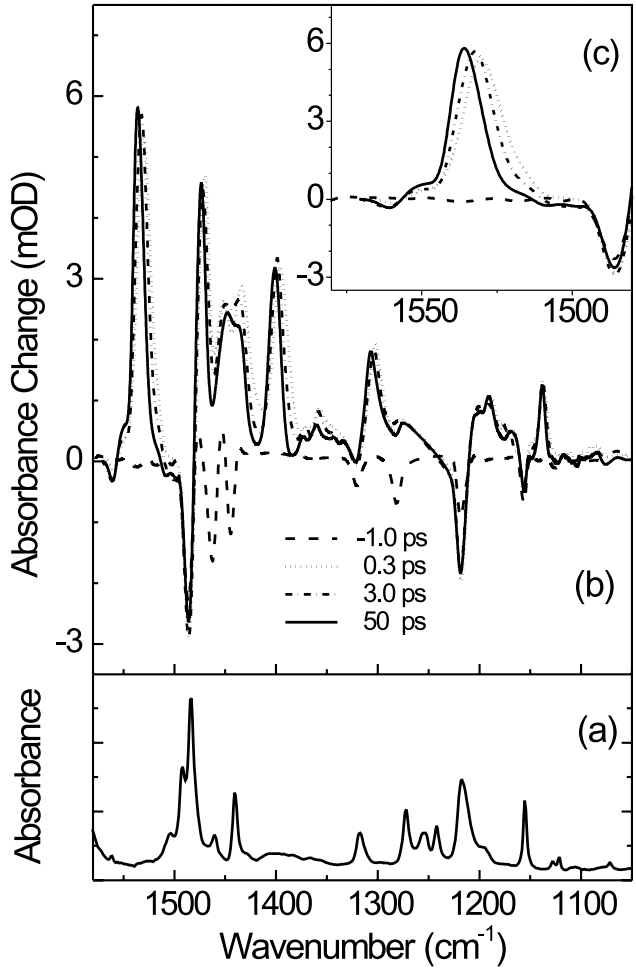

Figure 2 (*a*) IR spectrum of HBT in the fingerprint region. (*b*) Transient IR spectrum recorded at several pulse delays. (*c*) Expanded view showing frequency up-shift of the C=O marker band in the keto-S_1 state.

or higher lying states of the oscillator. In the latter case one expects a transient IR absorption on the $v = 1 \rightarrow 2$ transition of the oscillator that, owing to the diagonal anharmonicity of the mode, would appear red-shifted by 15–30 cm^{-1} with respect to the fundamental $v = 0 \rightarrow 1$ transition (99). Such an excited state absorption component is not observed in the transient spectra displaying exclusively the $v = 0 \rightarrow 1$ band. From the spectral width of the C=O band of 13 ± 2 cm^{-1} it is clear that even in a purely T_1-lifetime-dominated lineshape, the $v = 1$ state lifetime has a lower limit of 400 ± 50 fs. Absorption transients related to a $v = 1$ population

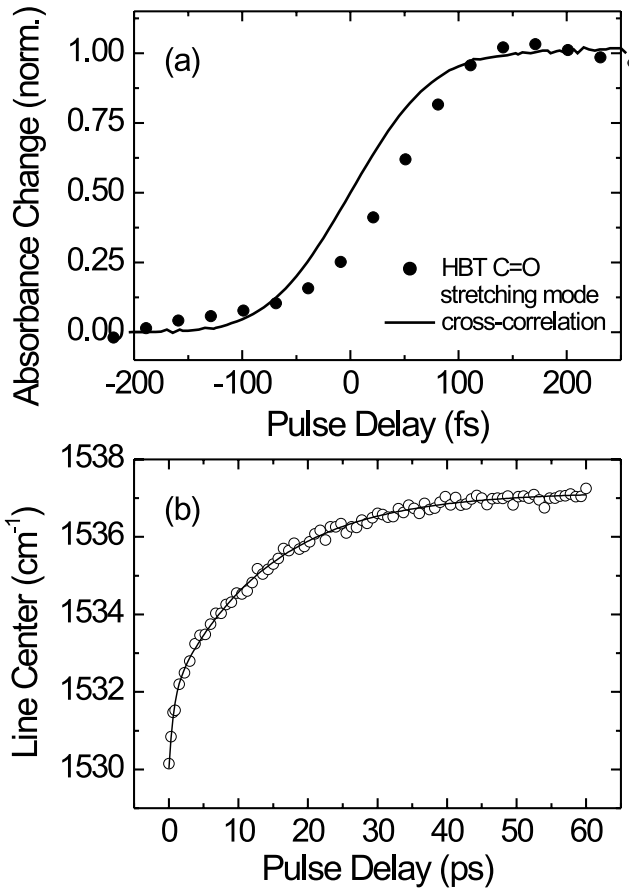

Figure 3 (*a*) Delayed rise of the C=O stretching band of HBT in the keto-S_1 state (*dots*, solvent signals substracted; *solid curve*, cross-correlation as recorded in ZnSe). (*b*) Transient frequency up-shift of the C=O band caused by intramolecular vibrational energy redistribution and cooling.

decay can thus easily be detected with a time resolution of 100 fs. The absence of signatures of $v = 1$ population suggests that the C=O vibration does not act as primary accepting mode driving the hydrogen transfer reaction by accepting (part of) the vibrational excess energy of about 3000 cm^{-1} released on transfer from enol to keto configuration. Similar to the behavior of the C=O stretching mode, all other observed IR-active fingerprint vibrations appear to be generated in their respective $v = 0$ states (24).

All IR-active vibrations in the fingerprint region show after initial appearance a blue-shift in transition frequency that can be fitted with two time constants ranging between 600–750 fs and 14–16 ps (23, 24) (see Figure 3). This spectral

shifting behavior is indicative of IVR and cooling processes, respectively, similar to that observed in other photoinduced chemical studies such as on azobenzene (66) or trans-stilbene (103). The transient spectra do not give direct insight into which anharmonically coupled modes cause the initial redshift. However, detailed steady-state resonance Raman of enol-HBT (112) and femtosecond UV/vis pump-probe studies (113) show the substantial displacement of a subset of low-frequency Raman-active vibrations in HBT. These modes are strongly elongated upon UV excitation, i.e., they acquire a significant nonequilibrium excitation. Upon femtosecond excitation some of these modes show coherent motions that last up to 2 ps. The observed blue-shift of the IR-active fingerprint vibrations then reflects the decrease of the excess population of these low-frequency Raman-active modes. It is interesting to note that the damping time $T_2 = 1$–2 ps of the coherent oscillations observed in femtosecond UV/vis pump-probe studies is about twice the fast component in the blue-shift representing IVR, as is expected for a dephasing dominated by population relaxation of excited vibrational levels (using the rule $1/T_2 = 1/(2T_1) + 1/T_2^*$, the pure dephasing rate is negligible $1/T_2^* \cong 0$).

4. BIMOLECULAR ACID-BASE PROTON TRANSFER REACTIONS

The neutralization reactions between Brønsted acids and bases in liquid solution are a prototype chemical reaction, as they provide insight into proton exchange phenomena such as autoionization in water (114), the von Grotthuss mechanism of high proton mobility in water (115), and proton pumps through membranes (116). In these reactions a proton is exchanged between the acid and the base:

$$\mathrm{RO{-}H + B \rightarrow RO^- + H{-}B^+}. \qquad 5.$$

Because these reactions are bimolecular, in liquid solution they are typically controlled by mutual diffusion (1). Eigen and Weller have established that for acid-base reactions in solutions, typical diffusion timescales are on the order of hundreds of picoseconds or longer. However, when an acid and a base do meet and form a reaction contact pair, the intrinsic on-contact reaction takes place with rates ranging from 10 ps^{-1} to 1 ps^{-1} (109, 117). Diffusion prevents a more refined insight of bimolecular reaction dynamics. The strategic approach to suppress the dominating role of diffusion is to investigate preformed complexes. In particular, proton transfer requires the formation of acid-base complexes, where the acid and base are connected via at least one hydrogen bond, which constitutes the proton transfer coordinate.

Proton transfer can be optically triggered by using a photoacid as proton donor. In a photoacid the electronic ground state has a low acidity (indicated by a large pK_a value; K_a is the acid dissociation equilibrium constant in water). Excitation to an electronic excited state having a larger acidity leads to a jump in pK_a value, typically by 4–6 units, thus facilitating an ultrafast optical triggering of the

proton transfer reaction. Photoacids have been studied since the pioneering work of Förster, Weller, and Eigen (109, 117, 118). Several classes of photoacids exist, most notably aromatic alcohols (phenols, naphthols, pyrenols) and protonated aminopyrenes (119–121).

Until now time-resolved studies, using time-correlated fluorescence single photon counting or UV/vis pump-probe spectroscopy, have investigated the proton transfer dynamics from the perspective of the photoacid (120). These studies provide in principle only direct insight into the dynamical process of proton dissociation from the photoacid by monitoring the decay of the photoacid S_1 state and/or the rise of the conjugated photobase S_1-species. These studies give insight into the proton transfer dynamics when the proton is directly scavenged by the accepting base. However, when the proton is first dissociating from the photoacid to the solvent, only to be taken up by an accepting base at later times, both the photoacid/conjugated photobase and the accepting base require monitoring. This is possible by following the dynamics of vibrational marker modes of the proton donating and the proton accepting species.

The acid-base neutralization reaction of pyranine (8-hydroxy-1,3,6-trisulfonate-pyrene; HPTS) with acetate (122, 123) in deuterated water recently has been investigated with femtosecond IR spectroscopy (25, 26). Here the vibrational marker modes were the HPTS photoacid band at 1493 cm^{-1} and the HPTS photobase band at 1503 cm^{-1} and the C=O stretching mode of acetic acid at 1720 cm^{-1}, which is formed upon deuteron pick-up by acetate. The decay of the HPTS photoacid and the rise of the HPTS photobase band indicate when the deuteron leaves the photoacid, whereas the rise of the acetic acid band specifies when the deuteron arrives at the deuteron accepting base.

By varying the concentration of the base acetate, and keeping the HPTS concentration fixed, several acid-base neutralization reaction schemes take place. It is known from previous studies that HPTS releases a deuteron to be solvated by the solvent D_2O with a time constant of 250 ps at room temperature (124). With the time-resolved IR experiment it has been demonstrated that for low acetate concentrations (<1 M) this solvated deuteron will be picked up by acetate at later times (25) (see Figure 4).

$$\underset{}{\mathrm{RO{-}D} + \mathrm{D_2O} + \mathrm{Ac^-} \rightarrow \mathrm{RO^-} + (\mathrm{D_3O})^+ + \mathrm{Ac^-} \rightarrow \mathrm{RO^-} + \mathrm{D_2O} + \mathrm{D{-}Ac}}$$
$$\underset{\text{solvated deuteron}}{\qquad\qquad\qquad} \qquad \underset{\text{full deuteron transfer}}{\qquad\qquad}$$

6.

For higher concentrations of acetate (>1 M) the relative encounter times between acetate and HPTS is short enough that a direct deuteron scavenging by the acetate base from the photoexcited HPTS dominates (125) (Figure 5). In the case of high base concentrations additional signal contributions to the rise of the C=O stretching mode are caused by preformed HPTS-acetate complexes.

$$\mathrm{RO{-}H \cdots B} \rightarrow \mathrm{RO^- \cdots H{-}B^+} \qquad 7.$$

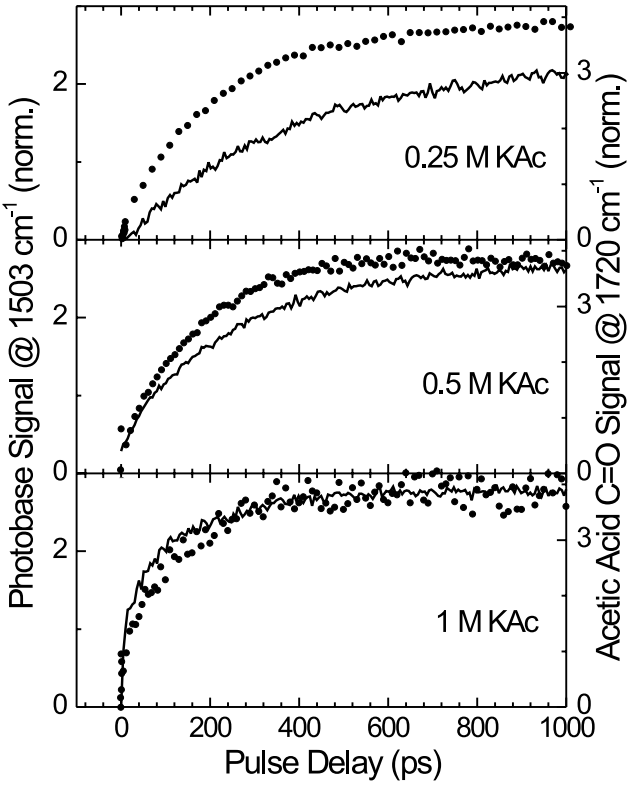

Figure 4 Comparison of the signal rise of the HPTS photobase band at 1503 cm^{-1} (*dots*) and the acetic acid marker mode at 1720 cm^{-1} (*solid lines*) at low base concentrations, indicating the initial deuteron release to the solvent and subsequent deuteron pick-up by the base.

The existence of these preformed complexes has been derived from electronic absorption band shifts (26), and from ultrafast components in the rise of the C=O stretching band of acetic acid, which makes up more than 50% of the total signal in 4 M acetate solutions (25).

The fraction of HPTS forming a preformed hydrogen-bonded tight complex with acetate transfers its deuteron within the time resolution of 150 fs. This hints at an essentially barrierless reaction coordinate for these tight HPTS-acetate complexes. In contrast the initially uncomplexed fraction of HPTS, which only reacts with acetate after mutual diffusion, has an on-contact reaction rate that is at least two orders of magnitude smaller (25). A superb correspondence between experimental and fitting results is obtained (26) when the Eigen-Weller model for acid-base neutralization, consisting of a diffusional stage and a reaction stage of tight complexes, is refined to include an additional reaction stage of loose complexes, presumably made of solvent separated HPTS and acetate (Figure 5).

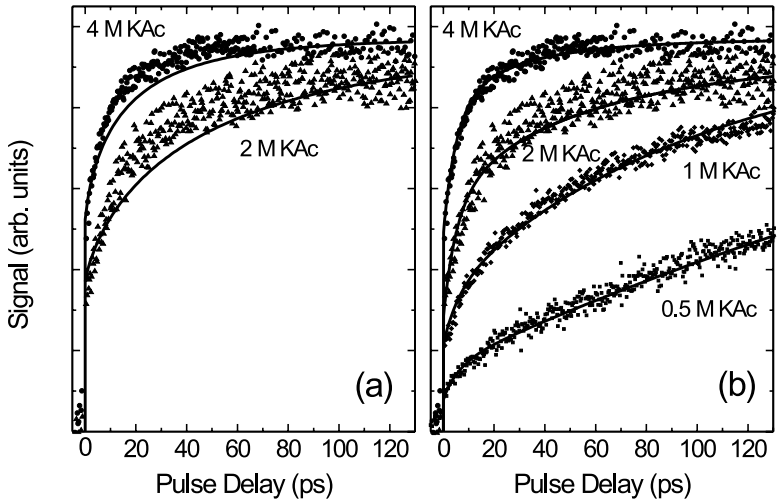

Figure 5 Concentration-dependent rise of the C=O stretching marker mode of acetic acid together with fitting results using (*a*) an instantaneous and a diffusion-controlled component (as published in Reference 25) and using (*b*) the three-component model with the additional static term caused by the loose complexes (26).

A possible reaction scheme involves two types of reactive complexes in sequential form:

$$\underset{\text{Diffusional Stage}}{\text{RO}-\text{D} + \text{Ac}^-} \rightarrow \underset{\substack{\text{Encounter Stage}\\ \text{loose complex}}}{\text{RO}-\text{D}\cdots(\text{D}_2\text{O})_n\cdots\text{Ac}^-} \rightarrow \underset{\substack{\text{Reaction Stage}\\ \text{tight complex}}}{\text{RO}-\text{D}\cdots\text{Ac}^- \rightarrow \text{RO}^-\cdots\text{D}-\text{Ac}} \quad 8.$$

In the Eigen-Weller model the dynamics are described by an unimolecular on-contact reaction rate k_r when the reactants have formed a contact pair after mutual diffusion (109, 117). In the Collins-Kimball approach (126) the diffusion-controlled reaction dynamics is determined by the von Smoluchowski equation for the time-dependent concentration of reactants at contact radius and the bimolecular finite reaction constant upon contact, k_0. The Collins-Kimball model was refined by Szabo with a Coulombic interaction potential between the reactants (127). Adding a second static term representing loose complexes in the fits of the experimental results allows for an experimental validation (26) of the connection between the diffusion-controlled reaction models of Eigen-Weller and of Collins-Kimball (128).

The initially uncomplexed HPTS molecules react with acetate with a bimolecular rate of $k_0 = 8 \cdot 10^{10}\ M^{-1}\ s^{-1}$. The reaction dynamics of the fraction of loose HPTS. . .acetate complexes already present at the moment of optical excitation of the photoacid can be described with a static unimolecular rate constant of $k_r = (6\ ps)^{-1}$, whereas the tight complexes have a static rate constant larger than $(150\ fs)^{-1}$. Rini et al. suggest that the relative slower proton transfer of the loose complexes is caused by more extensive solvent reorganization dynamics, e.g., when loose complexes first have to rearrange into tight complexes before the proton transfer from acid to base takes place (25). An alternative explanation might be that loose complexes transfer the deuteron through a water wire to the base in a von Grotthuss–type hopping mechanism (129). In the latter case the proton transfer rate is determined by the dynamical properties of the water wire.

5. ELECTRON TRANSFER

Electron transfer is an elementary chemical process of electronic charge redistribution between donor and acceptor groups. Photoinduced electron transfer plays a key role in the light harvesting in green plants, and in photovoltaic cells, where a light photon ultimately is converted into electrochemical energy. Electron transfer also plays a role in bimolecular reaction dynamics with the involvement of the harpooning mechanism. Bimolecular electron transfer between donor and acceptor molecules in solution is diffusion-controlled in the same manner as bimolecular proton transfer. However, the electron transfer reaction can take place with a rate that is distance dependent. In contrast, proton transfer is more likely to occur at a single on-contact distance, with the rate at zero at all other distances, in line with the von Smoluchowski and Collins-Kimball boundary conditions. Ultrafast intramolecular electron transfer dynamics has been shown to be often solvent controlled (130).

Ultrafast photoinduced electron transfer in the reaction centers of *Rhodobacter sphaeroides* has been followed by inspection of fingerprint vibrations of the special pair P, consisting of bacteriopheophytin H_A and quinone Q_A, revealing transfer and vibrational relaxation times (27–30). Intermolecular electron transfer from a dye, coumarin 337, to the solvent dimethylaniline has been studied through the C=C aromatic ring, and C=O and C≡N vibrations of the dye (131). Vibrational marker modes have been followed for electron injection in dye-sensitized nanocrystalline semiconductor films (36, 37). Here the metal-to-ligand charge transfer of Ru-complexes in solution has been compared to the transfer of Ru-complexes adsorbed on TiO_2, or ZrO_2 and SnO_2, and electron injection efficiencies have been determined. Polarization-sensitive probing of vibrational marker modes on a molecular system consisting of a zinc-porphyrin donor and a pyromellitic diimide acceptor connected by a spacer moiety has revealed the influence of the torsional angle between the donor and acceptors groups on electron transfer rates (39). A metal-to-ligand charge transfer reaction in a metallo-carbonyl compound has been

investigated by multidimensional IR spectroscopy after excitation with a UV pump. It has been found that specific CO vibrations can be labeled and then followed during the electron transfer process (38).

A prototype intramolecular charge transfer (ICT) reaction occurs in 4-dimethylaminobenzonitrile (DMABN). Here structural changes are supposed to take place when a locally excited (LE) state, reached by optical excitation, converts to an excited charge transfer (CT) state, responsible for the anomalously red-shifted fluorescence. The mechanisms that underlie the ICT of DMABN and related compounds have been subjects of an intense and long debate, fed by the experimental and theoretical results of a wide variety of techniques used to probe these compounds (132). Recent efforts in time-resolved vibrational spectroscopy on DMABN have focused on the identification of vibrational marker modes of the LE and CT states. In the rehybridization ICT (RICT) model a rehybridization of the cyano-group to a bend C=N geometry occurs (133). From initial femtosecond IR studies (31, 32) and theoretical predictions (134) the RICT model could be excluded, as this would imply a downshift of the C≡N mode to 1650 cm^{-1}, whereas it experimentally appears at 2100 cm^{-1}. Subsequent time-resolved IR (33, 34, 135) and resonance Raman studies (74–76) on several isotopomers of DMABN have focused on the identification of the ν(Ph-N) stretching mode. In the twisted ICT (TICT) model the charge redistribution is accompanied by a twisting of the dimethylamino from a conjugated planar configuration in the LE state to an electronically decoupled perpendicular ICT geometry (136). In the planar ICT (PICT) model the dimethylamino group changes from a pyramidalized LE state to a conjugated PICT state (137). For the TICT model the ν(Ph-N) stretching mode acquires more single-bond character and a downshift of 70 cm^{-1} has been calculated (134, 138), whereas for the PICT model an upshift of 47 cm^{-1} is the result of more double-bond character (134). Isotopic labeling has enabled the assignment of the ν(Ph-N) stretching mode to a band located at 1281 cm^{-1} in transient Raman experiments (75) and at 1276 cm^{-1} in transient IR measurements (34), from which an experimental downshift of 96 cm^{-1} compared to the ground state value has been determined. These results thus strongly favor the TICT model as the mechanism for the LE-CT conversion process. A full determination of the excited state structure based on this frequency shift, however, is not trivial, as the ν(Ph-N) stretching mode also involves motions of ring C–C stretching and C–H in-plane bending. It is noteworthy that in a recent TD-DFT calculation the structure of the CT state combines the twisted amino group conformation of TICT with the quinoidal ring structure of PICT (138).

Time-resolved resonance Raman spectroscopy has been applied to determine the population kinetics of Raman-active vibrations of betaine-30 (77) and p-nitroaniline (78, 79) that, after electronic excitation to the S_1 state with a large change in electronic charge distribution, respond with a prompt back electron transfer to the electronic ground state. Because of the large excess vibrational energy after this internal conversion process, large transient nonthermal populations can be determined, from which vibrational energy flow pathways can be derived.

From the obtained results it is has been concluded that the transient populations of the Raman-active modes do not follow a Boltzmann distribution on the earliest timescales. In the case of p-nitroaniline the primary accepting modes are combination/overtones of out-of-plane vibrations, rising with the internal conversion time constant of 0.5 ps, whereas the strong Raman active totally symmetric modes show a slower rise with a 2.5 ps time constant, followed by a 6 ps cooling behavior (79). Probing modes of p-nitroaniline in the IR give insight into timescales for IVR and cooling without revealing the IVR pathways (139). Evidence for vibrational excitation of C≡N stretching mode in back electron transfer in $(CN)_3FeCNRu(NH_3)_5^-$ has also been reported in a transient IR study (35).

6. HYDROGEN BONDING IN SOLVATION DYNAMICS

Solute-solvent interactions play a fundamental role in chemical reaction dynamics in liquids. To study these fluctuating interactions, electronic resonances of nonreactive molecules have been probed via the transient Stokes shift of fluorescence (4) and by coherent photon echo techniques (5–7). From these experiments the timescales of solvent fluctuations on (and solvent motions due to a change in) the electronic charge distribution in the solute can be obtained. These fluctuations lead to electronic coherence decay (optical dephasing) and spectral diffusion (solvation dynamics). One obtains, measured in time-resolved Stokes shift measurements, the solvation correlation function $S(t)$ (140):

$$S(t) = \frac{\omega_{el}(t) - \omega_{el}(\infty)}{\omega_{el}(0) - \omega_{el}(\infty)}, \qquad 9.$$

where $\omega_{el}(t)$ is the time-dependent electronic transition frequency between ground and excited state charge distributions. Within the linear response approximation $S(t)$ is identical to the electronic transition frequency fluctuation function $C(t)$, that is measured in electronic photon echo measurements:

$$C(t) = \frac{\langle \delta\omega_{el}(t)\ \delta\omega_{el}(0)\rangle}{\langle \delta\omega_{el}(0)^2\rangle}, \qquad 10.$$

where $\langle X\rangle$ denotes an ensemble average of the quantity X, and $\delta\omega_{el}$ denotes a fluctuation in the electronic energy difference $\delta\omega_{el} = \omega_{el} - \langle\omega_{el}\rangle$. In many cases, $C(t)$ consists of ultrafast (100–200 fs) and slower picosecond components. Molecular dynamics simulations have been extremely useful in elucidating that the degree and timescales of solvation depend not only on the solvent but also strongly on solute properties such as size, polarizability, charge distribution in ground and excited states, as well as solvent motion (141–144). From $C(t)$, however, it is not possible to obtain direct insight into nuclear coordinates, spatial dependencies, and specific local solute-solvent interactions. In particular, the degree of influence of site-specific hydrogen bonding on solvation dynamics has remained a relatively unexplored territory.

Site-specific excited state solute-solvent interactions have been probed with femtosecond IR spectroscopy on hydrogen-bonded complexes of the chromophore coumarin 102 (C102) (40–43, 145). Experiments on C102 complexed with the solvent chloroform and with phenol in the nonpolar solvent C_2Cl_4 have been performed. In the case of phenol as hydrogen donor both C102-phenol and C102-$(phenol)_2$ complexes have been probed. In the experiments the C=O stretching vibrational marker mode of C102 has been followed in time after electronic excitation with a UV-pump pulse tuned to the electronic origin transition around 400 nm. In the case of C102-$(phenol)_{1,2}$ complexes the O–H stretching band of the hydrogen donor phenol has also been probed.

C102 forms hydrogen bonds in the electronic ground state (Figure 6), as evidenced by the frequency downshift of 35 cm^{-1} of the C=O stretching mode in the case of C102 in $CHCl_3$ or C102-$(phenol)_{1,2}$. The broad O–H stretching band between 3200 and 3550 cm^{-1} indicates hydrogen-bonded hydroxyl groups, whereas the narrow peak at 3610 cm^{-1} is caused by uncomplexed phenol molecules. After electronic excitation a frequency up-shift of the C=O stretching band occurs within time resolution (<200 fs), from which it can be concluded that with the charge distribution of the S_1 state of C102 a hydrogen bond between C102 and

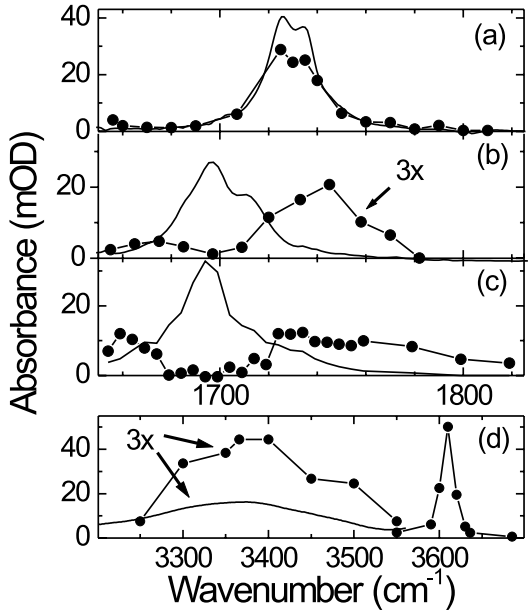

Figure 6 IR spectra of C102 in C_2Cl_4 (*a*), $CHCl_3$ (*b*), and complexed with phenol in C_2Cl_4 (*c*,*d*). The *solid lines* show the C=O and O–H stretching marker modes when C102 is in the electronic ground state, whereas the *dots* show the transient bands 0.5 ps after electronic excitation.

$CHCl_3$ or $(phenol)_{1,2}$ is energetically unfavorable and breaks within 200 fs. In the case of C102-$(phenol)_{1,2}$ the increase of signal at 3610 cm^{-1} is consistent with the estimated number of generated free O–H groups.

The C=O stretching mode is a sensitive probe to solvent shell rearrangements (40, 42, 43, 145) (see Figure 7). In the case of C102 dissolved in $CHCl_3$ a further frequency up-shift of 7 cm^{-1} has been observed. This vibrational Stokes shift $\Theta(t)$, with a 2.5 ps time constant, can be connected to the solvation correlation function $S(t)$ of Equation 9 and the frequency fluctuation correlation function $C(t)$ of Equation 10 (40, 42, 145). Adapting Pullin's derivation (146) for the

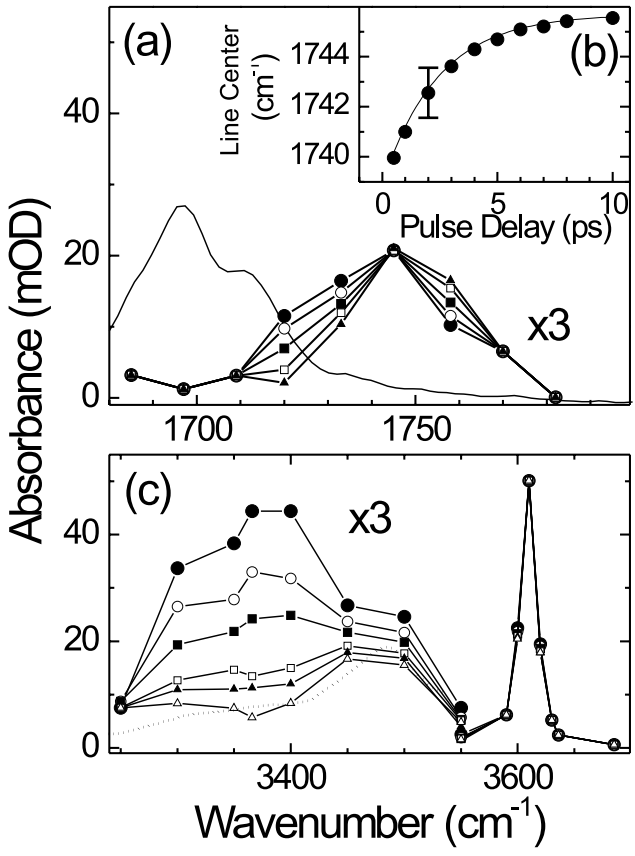

Figure 7 (*a*) Picosecond rearrangement dynamics of C102 (●: 0.5 ps; ○: 1 ps; ■: 2 ps; □: 4 ps; ▲: 10 ps), showing the vibrational Stokes shift in $CHCl_3$ of the C=O stretching mode around 1740 cm^{-1}. (*b*) The Stokes shift fits with a 2.5 ps time constant. (*c*) The broad O–H stretching band between 3200 and 3550 cm^{-1} of the released phenol-dimers (●: 0.4 ps; ○: 0.7 ps; ■: 1 ps; □: 1.5 ps; ▲: 2 ps; △: 5 ps) indicates a rearrangement to a configuration consistent with a free phenol-dimer (*dotted line*).

solvent-induced vibrational frequency shift $\Delta\tilde{\nu}_{sol}$ with a time-dependent reaction field for solute-solvent interaction, as defined by the van der Zwan-Hynes relation (147) for the solvation coordinate $z(t)$, it follows that

$$\Theta(t) = \frac{\Delta\tilde{\nu}_{sol}(t) - \Delta\tilde{\nu}_{sol}(\infty)}{\Delta\tilde{\nu}_{sol}(0) - \Delta\tilde{\nu}_{sol}(\infty)} = 1 - z(t) = S(t) \equiv C(t). \qquad 11.$$

The observed time constant for $\Theta(t)$ can be connected to the dielectric response function of the solvent. The experimentally found time constant for $\Theta(t)$ is consistent with results from earlier reported time-resolved fluorescence Stokes shift measurements (140). We note that Asbury et. al reported a similar derivation on the solvent-induced vibrational frequency shifts after electronic excitation of a metallo-carbonyl compound dissolved in several alcohols (148). The hydrogen bonding complex of C102 with aniline has also been monitored through its C=O stretching mode (44), revealing similar features.

In the case of the hydrogen-bonded complexes of C102-$(\text{phenol})_{1,2}$ a transient O–H stretching band between 3200–3550 cm^{-1} indicates a rearrangement having taken place with an 800 fs time constant (41–43). From a comparison of the transient IR spectra with the steady-state O–H stretching band of $(\text{phenol})_2$, it follows that the released phenol-dimer rearranges to its equilibrium configuration. This demonstrates again the potential of ultrafast vibrational spectroscopy of probing dynamics on both the hydrogen bond acceptor C102 and donor $(\text{phenol})_{1,2}$ sides. Electronic spectroscopic methods would only be able to probe the influence of the solvent motions affecting the dynamics of the chromophore C102.

These results show the importance of local hydrogen bond interactions and dynamics of solvated chromophores. Until now, it has been argued that these interactions have a minor impact on experimentally found correlation functions in time-dependent Stokes shift and photon echo measurements (149, 150). However, substantial solvent-induced shifts in electronic absorption and emission spectra are common for coumarin dyes when hydrogen bonds are formed (43, 151). It remains a task for future efforts to disentangle the magnitude of the influence of these hydrogen bond interactions on solvation dynamics. In this respect we also refer to recent gas-phase experiments on coumarin 151 clustered with hydrogen bond–donating solvent molecules (152).

Finally we note that besides probing local fingerprint modes, efforts have been undertaken to measure the low-frequency solvent modes directly in UV/vis-pump far-infrared-(THz)-probe spectroscopy. Until now results have been obtained only in the case of betaine-30 and p-nitroaniline (153, 154), where optical excitation induces large changes in electric dipole moments.

7. BOND FISSION

One of the most elementary photoinduced chemical processes is bond fission, where after absorption of a UV/vis photon one or several chemical bonds break and the molecular fragments separate from each other. Groundbreaking work on

photodissociation of small molecules using UV/vis pump-probe techniques has been reported since the early days of ultrafast spectroscopy (2). Following the dissociation reactions of small molecules in the IR on the other hand has been hampered by small absorption cross sections. Early examples include hydrogen abstraction by chlorine radicals (155) and vibrational product state dynamics of CN radical reactions in solution after photoexcitation of cyanogen iodide (17). Time-resolved resonance Raman spectroscopy has been applied to the dissociation and geminate recombination dynamics of OClO in solution (45, 47). Vibrational quantum beats led to the conclusion that the reaction dynamics is vibrationally mode specific (156). Interestingly, a transient isomer ClOO has been detected with this technique (46). Apart from a recent study on peptide conformational dynamics after cleavage of a disulfide bond (48), most time-resolved IR work has been done on metallo-carbonyl compounds, where dissociation, geminate recombination, and vibrational cooling have been studied (16, 18, 19, 55, 56). Rearrangements of the molecular fragments have also been observed (49–54) in a few cases supported by TD-DFT calculations (52, 53). An interesting line of research deals with the elucidation of light-triggered C–H bond activation of alkanes using organometallic complexes (57, 58, 60), later extended to C–Cl bonds and Si–H bonds (58, 59).

Heme proteins have a storage functionality for small ligands such as O_2, CO, and NO. These small ligands are attached to the central metal ion in the heme groups inside the proteins. Optical excitation leads to a metal-ligand bond cleavage, after which the small ligand can recombine, remain inside the protein pocket or leave the protein. Polarization sensitive UV/vis-pump IR-probe has been utilized to decipher the relative orientation of ligand to the heme metal, for the cases of CO myoglobin (20, 21, 61–63), CO hemoglobin (20–22, 62), and NO myoglobin (64). Quantum chemical calculations have shown that the transition vibrational dipole moment of the bound CO (95) or NO (64) ligand is not parallel to the bond vector of these ligands, and this should be taken into account when interpreting the polarization-sensitive experimental results. Despite much weaker signals the orientation of unbound CO located in the docking site has also been determined (61, 62). These results can be compared to recent time-resolved X-ray diffraction experiments (9). Picosecond resonance Raman spectroscopy has been used to investigate the IVR and cooling processes of the heme groups (80–82).

8. *cis-trans* ISOMERIZATIONS AND LARGER REARRANGEMENTS

An important class of photoinduced chemistry of organic molecules involves rearrangement along a double bond, usually referred to as *cis-trans* isomerization (157). Optically induced *cis-trans* isomerization is a key structural dynamical element for many types of photochromic switches (158) and for photosensor proteins (159). Time-resolved vibrational spectroscopy of optically-induced *cis-trans* isomerization has been reported on systems as diverse as azobenzene derivatives

(66, 69), all-*trans* retinal (67), retinal proteins such as bacteriorhodopsin (65, 68, 84–87), rhodopsin (88, 89), and photoactive yellow protein (70, 90).

A common feature in these *cis-trans* isomerization reactions is the ultrafast nature of the reaction dynamics taking place in a few picoseconds or less. Often optical excitation leads to formation of the isomerization product in its electronic ground state. Therefore a large amount of internal vibrational energy is present directly after isomerization. As a result, the vibrational fingerprint transitions appear often initially red-shifted because of off-diagonal anharmonic coupling with highly populated low-frequency modes, before vibrational cooling sets in on a timescale of several tens of picoseconds. Explicit examples include azobenzene in solution (66), azobenzene incorporated in a cyclic peptide (69), all-*trans* retinal in solution (67), and bacteriorhodopsin (65). In the latter case a transient IR experiment reported (68) the rise of a C–C stretching mode at 1190 cm^{-1} within 1 ps, from which the conclusion has been drawn that the all-*trans* to 13-*cis* configuration occurs already when the J state is formed with a 500 fs time constant. In contrast, from dedicated CARS experiments on a collection of artificial bacteriorhodopsin pigments with altered retinal chromophores (84–87), it has been argued that the *trans-cis* isomerization is not the first structural change to occur, but takes place during the J $\rightarrow$ K transformation on a picosecond timescale.

The combined ring-opening and *cis-trans* isomerization reaction of the spiropyran-merocyanine switch pair is one of the most studied photochromic reactions. Apart from time-resolved CARS studies on a spironaphthopyran compound (83) that demonstrated generation of the merocyanine product on a timescale of 25–50 ps, most subnanosecond time-resolved studies have used UV/vis-probing techniques (160). A recent effort to further elucidate the ultrafast photophysics of the spiropyrans 1′,3′,3′-trimethylspiro-[2H-1-benzopyran-2,2′-indoline] (BIPS) and its derivative 6-nitro-BIPS has been undertaken with femtosecond IR spectroscopy. The choice of solvent influenced not only which merocyanine isomers were formed (72), but also the efficiency of the rather influential internal conversion (IC) pathway causing the relaxation from excited BIPS (71) or 6-nitro-BIPS (72, 73) molecules back to the vibrationally cooled spiropyran electronic ground state; time constants ranged between 10 and 50 ps and an IC quantum yield ranged from 0.34 to 0.9 (Figure 8). The solvent-dependent quantum yield for this IC pathway was determined from analysis of the partial refilling of bleach signals at frequencies corresponding to vibrational absorptions of cold molecules in the electronic ground state, for a number of fingerprint modes (Figure 9). Transient absorptions, red-shifted from the cold spiropyran molecule vibrational absorption frequencies, were also observed and illustrated cooling of the hot spiropyran molecules in the electronic ground state.

IC is traditionally described using the energy gap law, which predicts a linear dependence of the logarithm of the IC rate on the energy gap separating (the minima of potential energy surfaces of) the electronic states involved in the internal conversion (161). The physical basis for the energy gap law is a rapid decrease of the Franck-Condon overlap with increasing vibrational quantum number. The

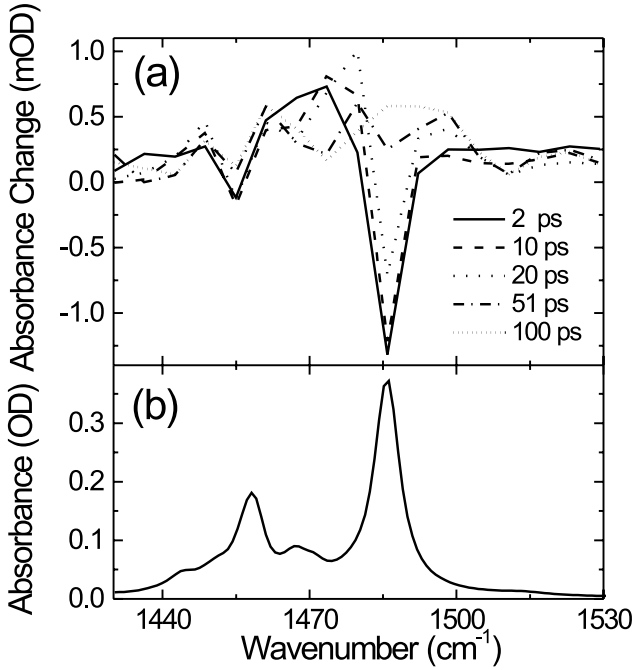

Figure 8 Transient IR spectra of BIPS in C_2Cl_4, recorded at several delays after UV excitation. The efficient IC to the electronic ground state of BIPS is clearly shown by the transient absorbance of hot BIPS between 1470 and 1485 cm $^{-1}$ observed at early pulse delays, followed by cooling with a 17 ps time constant, indicated by disappearance of the hot BIPS signals and the bleach recovery of the 1485 cm^{-1} band of cold BIPS. A merocyanine product band also appears in the same frequency region, as shown in the spectrum at 100 ps.

energy gap law has been experimentally verified for the $T_1 \rightarrow S_0$ transition of a series of hydrocarbons. Typical timescales for IC processes associated with the energy gap law are nanoseconds or longer. In recent years considerably faster IC rates were found for, e.g., DNA (162, 163) and green fluorescent protein (164, 165), which have been explained using the concept of conical intersections. For 6-nitro-BIPS the energy gap dependence, illustrated in Figure 9*a*, was found to be weaker than required on the basis of the energy gap law (73), while rise times of spiropyran hot bands and merocyanine product bands indicate that the IC process takes less than 10 ps, probably even less than a picosecond. The energy gap was modified because of variations in electrostatic interactions for different solvents. The results in Figure 9*a* disagreed with conventional understanding of the energy gap law, whereas the timescale of the IC process was in line with those ascribed to conical intersections. However, a theoretical analysis in the spirit of the energy gap law principle demonstrated that large energy gaps do not necessarily lead to small

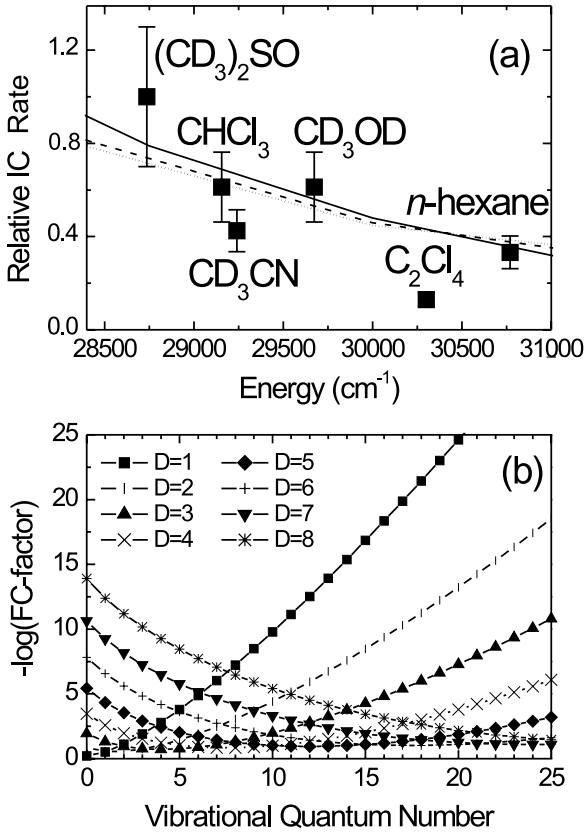

Figure 9 (*a*) Experimentally determined relative IC rates (■) for 6-nitro-BIPS versus the energy gap. The *lines* illustrate that the change of the Franck-Condon factor for transitions $v' = 0 \rightarrow v = n$ with increasing v can explain the observed trend. Fits are shown for three choices of vibrational energy hν, and corresponding required displacements D are h$\nu = 1250$ cm^{-1}, $D = 5.4$ (—); h$\nu = 2500$ cm^{-1}, $D = 3.3$ (- -); and h$\nu = 3750$ cm^{-1}, $D = 2.4$ ($\cdots$). The fits indicate that the data are in a regime where trends deviate from energy gap law behavior. (*b*) Logarithmic plot of the Franck-Condon factor for transitions between the excited state $v' = 0$ vibrational wavefunction and ground state vibrational wavefunctions for the vibrational quantum number $v = 0$–25 and displacements $D = 1$–8.

Franck-Condon factors (73). The key factor is the displacement between the potential energy surfaces. In fact, as illustrated in Figure 9*b*, for large displacements, which can be expected for (photo)chemical reactions, observed trends become more or less opposite to the energy gap law prediction. Interestingly, the theoretical analysis further showed that IC has the fastest rate, and thereby is often most efficient if the potential energy surface of the lower electronic state crosses through

the bottom of the surface of the higher electronic state (73), a condition that seems to support the relevance ascribed to conical intersections. The main conclusions are that the energy gap law is not generally valid, and that high IC quantum yields can be expected if an electronic excitation is accompanied by large conformational changes (73).

9. CONCLUSIONS AND PROSPECTS

The development of ultrafast IR and Raman spectroscopy has enabled a detailed insight into the dynamics of molecular structures during ultrafast chemical reactions. Probing specific vibrational marker modes provides site-specific information of particular chemical bonds. Excited state intramolecular hydrogen transfer in the prototype compound 2-(2′-hydroxyphenyl)benzothiazole has been demonstrated to occur on a timescale of 30–50 fs by inspection of the C=O stretching marker mode of the product keto-S_1 state. Hydrogen bonds of the solute chromophore coumarin 102 with hydrogen donors have been shown to cleave during solvent shell rearrangements induced by optical excitation. Bimolecular proton transfer between the photoacid pyranine and acetate in water has been monitored in different concentration regimes. At low base concentrations (<1 M) proton transfer to the solvent takes place before proton pick-up by the acetate base. Direct proton scavenging by the base occurs at higher base concentrations (>1 M). Comparison of proton transfer rates between directly complexed photoacid and base, and the on-contact rate of photoacid-base encounter complexes formed after mutual diffusion has necessitated a refinement of the traditional Eigen-Weller model for acid-base neutralization. Conversion between locally excited and charge transfer states of dimethylaminobenzonitrile have been monitored by transient IR and Raman spectroscopy. Comparison with ab initio quantum chemical calculations indicates the nature of these excited states. Polarization-sensitive spectroscopy has revealed the orientation of the CO or NO ligands in myoglobin or hemoglobin, either bound to the heme iron or released into the heme pockets.

Anharmonic coupling between vibrational normal modes leads to transient frequency shifts of vibrational transitions, when excess internal vibrational energy is present in the molecular systems. Intramolecular vibrational redistribution and vibrational cooling is reflected by the dynamical shifts of vibrational transitions as reported on, e.g., azobenzene and 2-(2′-hydroxyphenyl)benzothiazole. Ultrafast internal conversion to the electronic ground state has been monitored through transient red-shifted absorbance signals of hot molecules in the electronic ground state in the case of the photochromic switch 6-nitro-1′,3′,3′-trimethylspiro[2H-1-benzopyran-2,2′-indoline]. Subsequent decaying of these hot ground state signals and refilling of the bleach signals corresponding to cold molecules enable the estimation of the quantum yield of ground state recovery, that 6-nitro-1′,3′,3′-trimethylspiro-[2H-1-benzopyran-2,2′-indoline] has been found to be solvent dependent.

Future activities will include the application of polarization-sensitive spectroscopy on the reaction dynamics of more complex chemical transformations. Transient multidimensional vibrational spectroscopy will explore the structural information obtained from anharmonic couplings between vibrational normal modes. Developments in quantum chemical numerical procedures will enrich the potential of the method.

ACKNOWLEDGMENT

This review is the culmination of nine years of research, to whom we acknowledge the direct and indirect contributions by Georg Korn, Oliver Dühr, Christian Chudoba, Thomas Elsaesser, Frank Tschirschwitz, Andreas Kummrow, Jens Dreyer, Peter Hamm, Matteo Rini, Ben-Zion Magnes, Ann-Kathrin Holm, Karsten Heyne, Tomasz Zemojtel, Viivi Lehtovuori, Dina Pines, Omar F. Mohammed, and Anwar Usman.

LITERATURE CITED

1. Rice SA. 1985. *Diffusion-Limited Reactions*. Amsterdam: Elsevier
2. Zewail AH. 1988. *Science* 242:1645–53
3. Voth GA, Hochstrasser RM. 1996. *J. Phys. Chem.* 100:13034–49
4. Stratt RM, Maroncelli M. 1996. *J. Phys. Chem.* 100:12981–96
5. Nibbering ETJ, Duppen K, Wiersma DA. 1993. *Chem. Phys.* 183:167–85
6. Fleming GR, Cho M. 1996. *Annu. Rev. Phys. Chem.* 47:109–34
7. de Boeij WP, Pshenichnikov MS, Wiersma DA. 1998. *Annu. Rev. Phys. Chem.* 49:99–123
8. Kovalenko SA, Eilers-König N, Senyushkina TA, Ernsting NP. 2001. *J. Phys. Chem. A* 105:4834–43
9. Schotte F, Lim MH, Jackson TA, Smirnov AV, Soman J, et al. 2003. *Science* 300: 1944–47
10. Siwick BJ, Dwyer JR, Jordan RE, Miller RJD. 2003. *Science* 302:1382–85
11. Ruan C-Y, Lobastov VA, Vigliotti F, Chen SY, Zewail AH. 2004. *Science* 304:80–84
12. Plech A, Wulff M, Bratos S, Mirloup F, Vuilleumier R, et al. 2004. *Phys. Rev. Lett.* 92:125505
13. Cerullo G, De Silvestri S. 2003. *Rev. Sci. Instrum.* 74:1–18
14. Kaindl RA, Wurm M, Reimann K, Hamm P, Weiner AM, Woerner M. 2000. *J. Opt. Soc. Am. B* 17:2086–94
15. Elsaesser T, Kaiser W. 1986. *Chem. Phys. Lett.* 128:231–37
16. Moore JN, Hansen PA, Hochstrasser RM. 1989. *J. Am. Chem. Soc.* 111:4563–66
17. Raftery D, Gooding E, Romanovsky A, Hochstrasser RM. 1994. *J. Chem. Phys.* 101:8572–79
18. Dougherty TP, Heilweil EJ. 1994. *J. Chem. Phys.* 100:4006–9
19. Dougherty TP, Grubbs WT, Heilweil EJ. 1994. *J. Phys. Chem.* 98:9396–99
20. Moore JN, Hansen PA, Hochstrasser RM. 1988. *Proc. Natl. Acad. Sci. USA* 85: 5062–66
21. Hansen PA, Moore JN, Hochstrasser RM. 1989. *Chem. Phys.* 131:49–62
22. Anfinrud PA, Han C, Hochstrasser RM. 1989. *Proc. Natl. Acad. Sci. USA* 86: 8387–91

23. Rini M, Kummrow A, Dreyer J, Nibbering ETJ, Elsaesser T. 2003. *Faraday Discuss.* 122:27–40
24. Rini M, Dreyer J, Nibbering ETJ, Elsaesser T. 2003. *Chem. Phys. Lett.* 374: 13–19
25. Rini M, Magnes B-Z, Pines E, Nibbering ETJ. 2003. *Science* 301:349–52
26. Rini M, Pines D, Magnes B-Z, Pines E, Nibbering ETJ. 2004. *J. Chem. Phys.* 121:9593–610
27. Maiti S, Cowen BR, Diller R, Iannone M, Moser CC, et al. 1993. *Proc. Natl. Acad. Sci. USA* 90:5247–51
28. Maiti S, Walker GC, Cowen BR, Pippenger R, Moser CC, et al. 1994. *Proc. Natl. Acad. Sci. USA* 91:10360–64
29. Hamm P, Zurek M, Mantele W, Meyer M, Scheer H, Zinth W. 1995. *Proc. Natl. Acad. Sci. USA* 92:1826–30
30. Hamm P, Zinth W. 1995. *J. Phys. Chem.* 99:13537–44
31. Chudoba C, Kummrow A, Dreyer J, Stenger J, Nibbering ETJ, et al. 1999. *Chem. Phys. Lett.* 309:357–63
32. Kummrow A, Dreyer J, Chudoba C, Stenger J, Nibbering ETJ, Elsaesser T. 2000. *J. Chin. Chem. Soc.* 47:721–28
33. Okamoto H. 2000. *J. Phys. Chem. A* 104: 4182–87
34. Okamoto H, Inishi H, Nakamura Y, Kohtani S, Nakagaki R. 2001. *J. Phys. Chem. A* 105:4182–88
35. Wang CF, Mohney BK, Akhremitchev BB, Walker GC. 2000. *J. Phys. Chem. A* 104:4314–20
36. Heimer TA, Heilweil EJ, Bignozzi CA, Meyer GJ. 2000. *J. Phys. Chem. A* 104: 4256–62
37. Asbury JB, Ellingson RJ, Ghosh HN, Ferrere S, Nozik AJ, Lian T-Q. 1999. *J. Phys. Chem. B* 103:3110–19
38. Bredenbeck J, Helbing J, Hamm P. 2004. *J. Am. Chem. Soc.* 126:990–91
39. Rubtsov IV, Redmore NP, Hochstrasser RM, Therien MJ. 2004. *J. Am. Chem. Soc.* 126:2684–85
40. Chudoba C, Nibbering ETJ, Elsaesser T. 1998. *Phys. Rev. Lett.* 81:3010–13
41. Chudoba C, Nibbering ETJ, Elsaesser T. 1999. *J. Phys. Chem. A* 103:5625–28
42. Nibbering ETJ, Chudoba C, Elsaesser T. 1999. *Isr. J. Chem.* 39:333–47
43. Nibbering ETJ, Tschirschwitz F, Chudoba C, Elsaesser T. 2000. *J. Phys. Chem. A* 104:4236–46
44. Palit DK, Zhang TQ, Kumazaki S, Yoshihara K. 2003. *J. Phys. Chem. A* 107:10798–804
45. Hayes SC, Philpott MP, Mayer SG, Reid PJ. 1999. *J. Phys. Chem. A* 103:5534–46
46. Hayes SC, Thomsen CL, Reid PJ. 2001. *J. Chem. Phys.* 115:11228–38
47. Hayes SC, Wallace PM, Bolinger JC, Reid PJ. 2002. *Int. Rev. Phys. Chem.* 21:405–32
48. Volk M, Kholodenko Y, Lu HSM, Gooding EA, DeGrado WF, Hochstrasser RM. 1997. *J. Phys. Chem. B* 101:8607–16
49. George MW, Dougherty TP, Heilweil EJ. 1996. *J. Phys. Chem.* 100:201–6
50. Jiao TJ, Pang Z, Burkey TJ, Johnston RF, Heimer TA, et al. 1999. *J. Am. Chem. Soc.* 121:4618–24
51. Yeston JS, To TT, Burkey TJ, Heilweil EJ. 2004. *J. Phys. Chem. B* 108:4582–85
52. Yang H, Snee PT, Kotz KT, Payne CK, Harris CB. 2001. *J. Am. Chem. Soc.* 123:4204–10
53. Snee PT, Payne CK, Mebane SD, Kotz KT, Harris CB. 2001. *J. Am. Chem. Soc.* 123:6909–15
54. Owrutsky JC, Baronavski AP. 1996. *J. Chem. Phys.* 105:9864–73
55. Steinhurst DA, Baronavski AP, Owrutsky JC. 2002. *Chem. Phys. Lett.* 361:513–19
56. Lehtovuori V, Aumanen J, Myllyperkiö P, Rini M, Nibbering ETJ, Korppi-Tommola J. 2004. *J. Phys. Chem. A* 108:1644–49
57. Bromberg SE, Yang H, Asplund MC, Lian T, McNamara BK, et al. 1997. *Science* 278:260–63
58. Yang H, Kotz KT, Asplund MC, Wilkens MJ, Harris CB. 1999. *Acc. Chem. Res.* 32:551–60

59. Snee PT, Payne CK, Kotz KT, Yang H, Harris CB. 2001. *J. Am. Chem. Soc.* 123: 2255–64
60. Asplund MC, Snee PT, Yeston JS, Wilkens MJ, Payne CK, et al. 2002. *J. Am. Chem. Soc.* 124:10605–12
61. Lim M, Jackson TA, Anfinrud PA. 1995. *Science* 269:962–66
62. Lim M, Jackson TA, Anfinrud PA. 1995. *J. Chem. Phys.* 102:4355–66
63. Sagnella DE, Straub JE, Jackson TA, Lim M, Anfinrud PA. 1999. *Proc. Natl. Acad. Sci. USA* 96:14324–29
64. Zemojtel T, Rini M, Heyne K, Dandekar T, Nibbering ETJ, Kozlowski PM. 2004. *J. Am. Chem. Soc.* 126:1930–31
65. Diller R, Iannone M, Cowen BR, Maiti S, Bogomolni RA, Hochstrasser RM. 1992. *Biochemistry* 31:5567–72
66. Hamm P, Ohline SM, Zinth W. 1997. *J. Chem. Phys.* 106:519–29
67. Hamm P, Zurek M, Roschinger T, Patzelt H, Oesterhelt D, Zinth W. 1997. *Chem. Phys. Lett.* 268:180–86
68. Herbst J, Heyne K, Diller R. 2002. *Science* 297:822–25
69. Bredenbeck J, Helbing J, Behrendt R, Renner C, Moroder L, et al. 2003. *J. Phys. Chem. B* 107:8654–60
70. Groot ML, van Wilderen LJGW, Larsen DS, van der Horst MA, van Stokkum IHM, et al. 2003. *Biochemistry* 42:10054–59
71. Rini M, Holm A-K, Nibbering ETJ, Fidder H. 2003. *J. Am. Chem. Soc.* 125: 3028–34
72. Holm A-K, Rini M, Nibbering ETJ, Fidder H. 2003. *Chem. Phys. Lett.* 376:214–19
73. Fidder H, Rini M, Nibbering ETJ. 2004. *J. Am. Chem. Soc.* 126:3789–94
74. Kwok WM, Ma C, Phillips D, Matousek P, Parker AW, Towrie M. 2000. *J. Phys. Chem. A* 104:4188–97
75. Kwok WM, Ma C, Matousek P, Parker AW, Phillips D, et al. 2001. *J. Phys. Chem. A* 105:984–90
76. Ma C, Kwok WM, Matousek P, Parker AW, Phillips D, et al. 2002. *J. Phys. Chem. A* 106:3294–305
77. Hogiu S, Werncke W, Pfeiffer M, Dreyer J, Elsaesser T. 2000. *J. Chem. Phys.* 113:1587–94
78. Kozich V, Werncke W, Dreyer J, Brzezinka KW, Rini M, et al. 2002. *J. Chem. Phys.* 117:719–26
79. Kozich V, Werncke W, Vodchits AI, Dreyer J. 2003. *J. Chem. Phys.* 118:1808–14
80. Mizutani Y, Kitagawa T. 1997. *Science* 278:443–46
81. Nakashima S, Taniguchi S, Okada T, Osuka A, Mizutani Y, Kitagawa T. 1999. *J. Phys. Chem. A* 103:9184–89
82. Mizutani Y, Kitagawa T. 2001. *J. Phys. Chem. B* 105:10992–99
83. Aramaki S, Atkinson GH. 1992. *J. Am. Chem. Soc.* 114:438–44
84. Ujj L, Zhou Y-D, Sheves M, Ottolenghi M, Ruhman S, Atkinson GH. 2000. *J. Am. Chem. Soc.* 122:96–106
85. Atkinson GH, Ujj L, Zhou YD. 2000. *J. Phys. Chem. A* 104:4130–39
86. Atkinson GH, Zhou Y, Ujj L, Aharoni A, Sheves M, Ottolenghi M. 2002. *J. Phys. Chem. A* 106:3325–36
87. Terentis AC, Zhou YD, Atkinson GH, Ujj L. 2003. *J. Phys. Chem. A* 107:10787–97
88. Popp A, Ujj L, Atkinson GH. 1996. *Proc. Natl. Acad. Sci. USA* 93:372–76
89. Jäger F, Lou J-H, Nakanishi K, Ujj L, Atkinson GH. 1998. *J. Am. Chem. Soc.* 120:3739–47
90. Zhou Y, Ujj L, Meyer TE, Cusanovich MA, Atkinson GH. 2001. *J. Phys. Chem. A* 105:5719–26
91. Nibbering ETJ, Elsaesser T. 2004. *Chem. Rev.* 104:1887–914
92. Koch W, Holthausen MC. 2001. *A Chemist's Guide to Density Functional Theory*. Weinheim, Germany: Wiley-VCH
93. Roos BO, Andersson K, Fulscher MP, Malmqvist P-Å, Serrano-Andrés L, et al. 1996. *Adv. Chem. Phys.* 93:219–331

94. Marques MAL, Gross EKU. 2004. *Annu. Rev. Phys. Chem.* 55:427–55
95. Spiro TG, Kozlowski PM. 1998. *J. Am. Chem. Soc.* 120:4524–25
96. Hadži D, Bratos S. 1976. In *The Hydrogen Bond: Recent Developments in Theory and Experiments*, ed. P Schuster, G Zundel, C Sandorfy, pp. 565–611. Amsterdam: North-Holland
97. Herzberg G. 1945. *Molecular Spectra and Molecular Structure. II. Infrared and Raman Spectra of Polyatomic Molecules*. New York: Van Nostrand
98. Nielsen HH. 1951. *Rev. Mod. Phys.* 23: 90–136
99. Hamm P, Hochstrasser RM. 2001. In *Ultrafast Infrared and Raman Spectroscopy*, ed. MD Fayer, pp. 273–347. New York: Marcel Dekker
100. Gruebele M. 2000. *Adv. Chem. Phys.* 114:193–261
101. Elsaesser T, Kaiser W. 1991. *Annu. Rev. Phys. Chem.* 42:83–107
102. Owrutsky JC, Raftery D, Hochstrasser RM. 1994. *Annu. Rev. Phys. Chem.* 45: 519–55
103. Iwata K, Hamaguchi H. 1997. *J. Phys. Chem. A* 101:632–37
104. Wynne K, Hochstrasser RM. 1995. *Chem. Phys.* 193:211–36
105. Hamm P. 1995. *Chem. Phys.* 200:415–29
106. Chachisvilis M, Fidder H, Sundström V. 1995. *Chem. Phys. Lett.* 234:141–50
107. Towrie M, Parker AW, Shaikh W, Matousek P. 1998. *Meas. Sci. Technol.* 9: 816–23
108. Matousek P, Towrie M, Stanley A, Parker AW. 1999. *Appl. Spectrosc.* 53:1485–89
109. Weller A. 1961. *Progr. React. Kinet.* 1: 187–213
110. Klöpffer W. 1977. *Adv. Photochem.* 10:311–58
111. Elsaesser T. 2002. See Ref. 166, pp. 119–53
112. Pfeiffer M, Lenz K, Lau A, Elsaesser T, Steinke T. 1997. *J. Raman Spectrosc.* 28:61–72
113. Lochbrunner S, Wurzer AJ, Riedle E. 2003. *J. Phys. Chem. A* 107:10580–90
114. Geissler PL, Dellago C, Chandler D, Hutter J, Parrinello M. 2001. *Science* 291:2121–24
115. Marx D, Tuckerman ME, Hutter J, Parrinello M. 1999. *Nature* 397:601–4
116. Luecke H, Lanyi JK. 2003. *Adv. Protein Chem.* 63:111–30
117. Eigen M. 1964. *Angew. Chem. Int. Ed.* 3:1–19
118. Förster T. 1950. *Z. Elektrochem.* 54:531–35
119. Tolbert LM, Solntsev KM. 2002. *Acc. Chem. Res.* 35:19–27
120. Pines E, Pines D. 2002. See Ref. 166, pp. 155–84
121. Pines E. 2003. In *Chemistry of Phenols*, ed. Z Rappoport, pp. 491–529. New York: Wiley
122. Pines E, Magnes BZ, Lang MJ, Fleming GR. 1997. *Chem. Phys. Lett.* 281:413–20
123. Genosar L, Cohen B, Huppert D. 2000. *J. Phys. Chem. A* 104: 6689–98
124. Pines E, Huppert D, Agmon N. 1988. *J. Chem. Phys.* 88:5620–30
125. Goldberg SY, Pines E, Huppert D. 1992. *Chem. Phys. Lett.* 192:77–81
126. Collins FC, Kimball GE. 1949. *J. Colloid Sci.* 4:425–37
127. Szabo A. 1989. *J. Phys. Chem.* 93:6929–39
128. Shoup D, Szabo A. 1982. *Biophys. J.* 40:33–39
129. Tanner C, Manca C, Leutwyler S. 2003. *Science* 302:1736–39
130. Barbara PF, Walker GC, Smith TP. 1992. *Science* 256:975–81
131. Wang CF, Akhremitchev B, Walker GC. 1997. *J. Phys. Chem. A* 101:2735–38
132. Grabowski ZR, Rotkiewicz K, Rettig W. 2004. *Chem. Rev.* 103:3899–4031
133. Sudholt W, Sobolewski AL, Domcke W. 1999. *Chem. Phys.* 240:9–18
134. Dreyer J, Kummrow A. 2000. *J. Am. Chem. Soc.* 122:2577–85

135. Okamoto H, Kinoshita M, Kohtani S, Nakagaki R, Zachariasse KA. 2002. *Bull. Chem. Soc. Jpn.* 75:957–63
136. Rotkiewicz K, Grellmann KH, Grabowski ZR. 1973. *Chem. Phys. Lett.* 19:315–18
137. Zachariasse KA, Grobys M, von der Haar T, Hebecker A, Ilichev YV, et al. 1996. *J. Photochem. Photobiol. A* 102:59–70
138. Rappoport D, Furche F. 2004. *J. Am. Chem. Soc.* 126:1277–84
139. Schrader T, Sieg A, Koller F, Schreier W, An Q, et al. 2004. *Chem. Phys. Lett.* 392:358–64
140. Horng ML, Gardecki JA, Maroncelli M. 1997. *J. Phys. Chem. A* 101:1030–47
141. Kumar PV, Maroncelli M. 1995. *J. Chem. Phys.* 103:3038–60
142. Ando K. 1997. *J. Chem. Phys.* 107:4585–96
143. Cichos F, Brown R, Bopp PA. 2001. *J. Chem. Phys.* 114:6824–33
144. Cichos F, Brown R, Bopp PA. 2001. *J. Chem. Phys.* 114:6834–42
145. Nibbering ETJ, Elsaesser T. 2000. *Appl. Phys. B* 71:439–41
146. Pullin ADE. 1958. *Spectrochim. Acta* 13:125–38
147. van der Zwan G, Hynes JT. 1985. *J. Phys. Chem.* 89:4181–88
148. Asbury JB, Wang YQ, Lian T-Q. 2002. *Bull. Chem. Soc. Jpn.* 75:973–83
149. Moog RS, Bankert DL, Maroncelli M. 1993. *J. Phys. Chem.* 97:1496–501
150. Chapman CF, Fee RS, Maroncelli M. 1995. *J. Phys. Chem.* 99:4811–19
151. Tschirschwitz F, Nibbering ETJ. 1999. *Chem. Phys. Lett.* 312:169–77
152. Chen Y, Palmer PM, Topp MR. 2002. *Int. J. Mass Spectrom.* 220:231–51
153. Haran G, WeiDong S, Wynne K, Hochstrasser RM. 1997. *Chem. Phys. Lett.* 274:365–71
154. McElroy R, Wynne K. 1997. *Phys. Rev. Lett.* 79:3078–81
155. Raftery D, Iannone M, Phillips CM, Hochstrasser RM. 1993. *Chem. Phys. Lett.* 201:513–20
156. Fidder H, Tschirschwitz F, Dühr O, Nibbering ETJ. 2001. *J. Chem. Phys.* 114:6781–94
157. Dugave C, Demange L. 2003. *Chem. Rev.* 103:2475–532
158. Feringa BL, ed. 2001. *Molecular Switches*. Weinheim, Germany: Wiley-VCH
159. Gai F, Hasson KC, McDonald JC, Anfinrud PA. 1998. *Science* 279:1886–91
160. Minkin VI. 2004. *Chem. Rev.* 104:2751–76
161. Michl J, Bonacic-Koutecký V. 1990. *Electronic Aspects of Organic Photochemistry*. New York: Wiley-Intersci.
162. Pecourt J-ML, Peon J, Kohler B. 2001. *J. Am. Chem. Soc.* 123:10370–78
163. Crespo-Hernández CE, Cohen B, Hare PM, Kohler B. 2004. *Chem. Rev.* 104:1977–2019
164. Webber NM, Litvinenko KL, Meech SR. 2001. *J. Phys. Chem. B* 105:8036–39
165. Mandal D, Tahara T, Meech SR. 2004. *J. Phys. Chem. B* 108:1102–8
166. Elsaesser T, Bakker HJ, eds. 2002. *Ultrafast Hydrogen Bonding Dynamics and Proton Transfer Processes in the Condensed Phase.* Dordrecht: Kluwer Acad.

Annual Review of Physical Chemistry
Volume 56, 2005

CONTENTS